Spider (*Linothele megatheloides)* and silkworm *(Bombyx mori)* silks: Comparative physical and biological evaluation

Yuejiao Yang[a,b,1], Gabriele Greco[c,d,1], Devid Maniglio[a,b], Barbara Mazzolai[d], Claudio Migliaresi[a,b], Nicola Pugno[c,e,f,**], Antonella Motta[a,b,*]

[a] *Department of Industrial Engineering and BIOtech Research Center, University of Trento, Trento, Italy*
[b] *European Institute of Excellence on Tissue Engineering and Regenerative Medicine, Trento Unit, Trento, Italy*
[c] *Laboratory of Bio-Inspired & Graphene Nanomechanics, Department of Civil, Environmental and Mechanical Engineering, University of Trento, Italy*
[d] *Center for Micro-BioRobotics@SSSA, Istituto Italiano di Tecnologia, Italy*
[e] *School of Engineering and Materials Science, Queen Mary University of London, United Kingdom*
[f] *Ket-Lab, Edoardo Amaldi Foundation, Italy*

ARTICLE INFO

ABSTRACT

Silks, in particular silkworm silks, have been studied for decades as possible candidate materials for biomedical applications. Recently, great attentions have been paid to spider silks, mainly due to their unique and remarkable mechanical properties. Both materials express singular interactions with cells through specific biorecognition moieties on the core proteins making up the two silks. In this work, the silk from a Colombian spider, *Linothele megatheloides* (LM), which produces a single type of silk in a relatively large amount, was studied in comparison with silk from *Bombyx mori* silkworm, before and after degumming, with the evaluation of their chemical, mechanical and biological properties. Unexpected biological features in cell culture tests were found for the LM silk already at very early stage, so suggesting further investigation to explore its use for tailored biomedical applications.

1. Introduction

Silk fibers produced by silkworms [1] and spiders [2] have aroused great interests among researchers during the past decades due to their unique properties [3,4]. The natural silk fiber produced by silkworm has been deeply studied and used/proposed for biomedical applications such as tissue engineering, prosthetic material and drug delivery [5–9]. Also spider silk nowadays is taken into consideration for biomedical applications [10]. Spiders use silk to build robust cobwebs [11,12] and also for making egg sacks [13], lifting heavy objects [14] and even flying [15]. For each specific function, composition and properties of the silk filaments are different and this is a crucial difference with respect to the silkworm silk, which has single chemical composition and properties [16]. Among the different types of spider silk that exist on Earth (which are estimated to be 150,000), only dragline silk (mainly from *Nephila clavipes*), which composes the main frame of the web, has been intensively studied and characterized in terms of physical,

chemical and biological properties [17].

Allmeling C. et al. [18] used the dragline silk of the spider of the genus *Nephila* to make constructs that were seeded with Schwann cells and were investigated as sciatic nerve conduits in rats. They concluded that native dragline silk is a viable material for Schwann cell migration and proliferation for peripheral nerve regeneration. Vollrath F. et al. [19] proved the biocompatibility of major ampullate dragline silk reeled from *Nephila clavipes*, native silk reeled from a *Brachypelma sp.* spider, and native silk taken from this spider's web, implanted subcutaneously in pigs. In these works, after the epicutaneous application of the material, a rapid healing process was observed superficially and after 14 days histopathological analysis revealed no difference between the original and the newborn tissue. However, the main challenge of applying native dragline silk in tissue engineering is the low scale production and the spiders' cannibalistic behavior [20] that make it difficult farming spiders and harvesting their silk. Production of spider silk-like fiber through modified organisms has been investigated for

---

decades, with genetically modified plants [21], mammals [22], silkworm [23], yeast and bacteria, to have alternative more exploitable sources of this remarkable protein [24]. With all investigated methods, however, silks structurally similar but with inferior properties with respect to the ones spun by the spiders were obtained [25].

Recent improvement in spinning technology has been achieved thanks to the work of Rising and Johannson [26,27]. In particular, they produced a large-scale amount of spider silk-like fibers by using a biomimetic apparatus with pH gradient and shear forces, as it occurs in the natural spinning dope of spiders. However, the mechanical properties of these fibers were still poor with respect to the natural ones. In this regards, the work of Bowen et al. [25] demonstrated that is possible to improve the mechanical properties of spider artificial silk by increasing the molecular weight of the spun proteins. However, in spite of the many brilliant results, we are still far from scalability of these materials with properties close to those of the native spider silk. For this reason, a further and deeper investigation on new possible raw silks has to be done. Then, solutions or alternative to the artificial spinning, with better scalability and properties could be discovered and explored.

In this work, we studied for the first time the silk produced by one of the largest Dipluridae spiders original from Colombia, *Linothele megatheloides* (Paz & Raven, 1990) [28] (Fig. 1a). The peculiarity of these spider is in its two 2 cm long spinnerets, the large up to 60 mg amount of silk produced in a week, and the easiness to farm with respect to other orb weaver spiders (Fig. 1b) [29]. Furthermore, this species produces only one type of silk, this leading to a simplification of the silk-harvesting process (Fig. 1c) [30]. Mechanical properties, fiber morphology, protein structure and amino acid composition of *Linothele megatheloides* spider (LM) silk were characterized and compared with silk from *Bombyx mori* cocoon before (SC) and after degumming (DS). Preliminary biocompatibility aspects of natural networks made by different types of silk mentioned above were studied by imaging cell (NIH 3T3 fibroblast) adhesion with confocal microscopy, and assessing cells metabolic activity and proliferations. Competitive cell adhesion test was assessed by directly comparison of LM silk and *Bombyx mori* silk (before and after degumming).

2. Materials and methods

2.1. Materials

Spiders under study were adult females of *Linothele megatheloides* (Aranae, Paz & Raven, 1990). One of the reasons to choose this specie was that the easy possibility to extract the silk without damaging it. They were kept in different glass or plastic terrariums and fed with a weekly diet of insects (mainly *Blaptica dubia* or *Acheta domestica*). All the terrariums were set in a room with controlled environmental parameters. Each terrarium was provided with a small refuge by considering the need of the spider to feel protect and live without stress, according to the Italian regulation on animal protection and EU Directive 2010/63/EU for animal experiments. *Bombyx mori*

(polyhybrid) cocoons, produced in a controlled environment, were kindly provided by Chul Thai Silk Co., Ltd. (Petchaboon province, Thailand). Undegummed and degummed fibers were considered. For degumming, cocoons were cut in to pieces and then treated in two 98 °C distilled (DI) water baths of Na_2CO_3 (Sigma, USA, 1.1 g/L and 0.4 g/L, respectively), 1.5 h each, 10 g per liter. Then they were rinsed thoroughly with warm DI water to remove the salt and completely dried at room temperature in a laminar flow hood.

2.2. Sample preparation

For cell proliferation and metabolic activity tests, round samples 1.5 cm diameter were isolated from the original silk net of the spider and from a thin layer separated from the middle part of the cocoon, without (SC) and after (DS) degumming.

For cell adhesion test, fibers were isolated from the net samples and competitively tested in couples fixed on a polymethylmethacrylate frame (Fig. S1).

2.3. Field Emission Scanning Electron Microscopy (FE-SEM) observations

Samples with cells were first fixed in 4% glutaraldehyde in 0.1 M Cacodylate buffer for 1 h at room temperature, followed by washing in 0.1 M cacodylate buffer (three times) and then dried at room temperature. All samples were observed with a field emission-scanning electron microscope (FE-SEM, Supra 40/40VP, Zeiss, Germany), in dry state and after coating with Pt/Pd in a reduced argon atmosphere.

2.4. Mechanical properties

The tested samples were prepared by following the same procedure reported by Blackledge et al. [31]. We stuck the silk samples on a paper frame provided with a square window of 1 cm side. The silk sample was fixed to the paper frame with a double-sided tape. For silkworm silk it was sufficient to collect the single thread spun by the spider. On the other hand, for the silk of *Linothele megatheloides* we stimulate directly the spinneret of the spider to stimulate the spinning of the silk. For the mechanical characterization, we used a nanotensile machine (Agilent technologies T150 UTM) with a cell load of 500 mN. The imposed strain rate was 1%/s. Before mounting the samples, we measured their diameter with an optical microscope. The declared sensitivity of the machine is 10 nN for the load and 0.1 nm for the displacement in the dynamic configuration. Ten samples were tested for each silk type and we report the mean value and standard deviation. The tensile tests were performed at a temperature of 21 °C and relative humidity of 35–39%. In this work we did not tested the silks at different humidity rates. Moreover, a quite recent work on supercontraction (effect of humidity on spider silk mechanical and structural properties) on suborder of Mygalomorphae spiders suggested that the effect of humidity on their silks is minimal when compared to those of orb weavers [32].
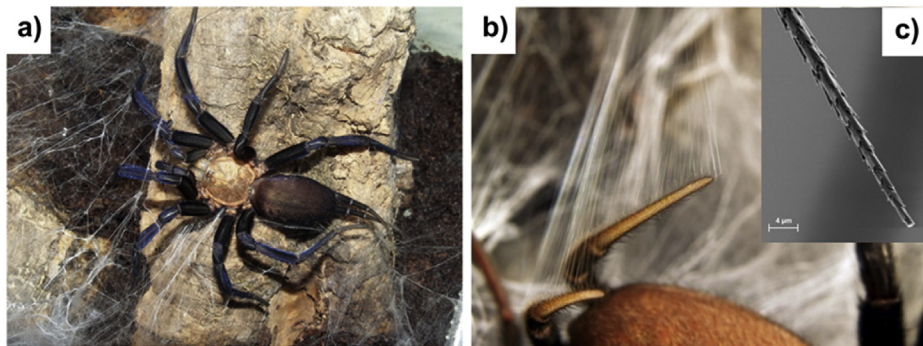

Fig. 1. *Linothele megatheloides* spider (LM) and its spigots. a) The Colombian spider *Linothele megatheloides* (frontal view, Courtesy of Enrico Simeon); b) The spinneret of LM spider (Courtesy of Enrico Simeon); c) Field Emission Scanning Electron Microscopy (FE-SEM) image of the spigots on spinnerets of LM spider. The scale bar in figure c is equivalent to 4 μm.

2.5. Atomic Force Microscopy (AFM)

The AFM used to obtain the images, topography and force curves on the samples is a NT-MDT Smena scanner. The environmental conditions at which we operated were controlled and with a temperature of 24 °C and relative humidity of 71%. We used different cantilevers and operational modalities to obtain topography and force curves respectively. The former was measured in semi-contact mode, by using a NT-MTD NSG-11B tip (10 nm nominal tip radius, resonance frequency of 181 kHz and force constant between 2.5 and 10 N/m). The latter were obtained by using a contact mode tip (NT-MTD, CSG-11B, 10 nm nominal tip radius, 428 kHz resonance frequency and force constant between 0.01 and 0.08 N/m).

The threads of the different silks type were stuck in a Double-Sided Bonding tape on the sapphire AFM sample holder. AFM data were analyzed with the support of Gwyddion and IA_P9 application. The roughness values were computed both for the average (Ra) and mean root square (Rq) value, following British standard ISO 4287:2000.

The current/tip-deflection response curve of the cantilever was calculated starting from the current/distance curves collected on a silicon chip surface and was estimated to be equal to 0.006 A/m. The adhesion force values where obtained by using the nominal elastic constant of the used cantilevers and by measuring the jump out current of the tip from the surfaces of the silk. Ten curves were obtained for each type of silk. Mean and standard deviation of the snap-out current values were then computed.

2.6. Fourier transformation infrared spectroscopy (FTIR)

Fourier transformation infrared spectroscopy (FTIR) analysis was performed directly on LM silk in attenuated total reflectance (ATR) mode (FTIR–ATR, Spectrum One, PerkinElmer, USA) equipped with Zinc Selenide crystal on ATR. The spectrum collected in the range from 650 to 4000 cm^{-1} with 64 scans at the resolution of 4 cm^{-1}. Secondary structures analysis of protein structure were determined by Fourier transform infrared spectroscopy (FTIR) in attenuated total reflectance (ATR) mode (FTIR–ATR, Spectrum One, PerkinElmer, USA) equipped with Zinc Selenide crystal on ATR. The spectra processing was performed by Origin 2016 software (peak analyzer mode). The spectra were baseline corrected, smoothed with the Savitsky-Golay method (10 points). A Fourier self-deconvolution (FSD, parameter setting: Gamma 5 and Smoothing Factor 0.2) was used to enhance of the infrared spectra in the Amide I region (1600 - 1700 cm^{-1}) [31]. Then the peaks assigned to different secondary structures [31] were determined using a second order derivative and fitted using Gaussian function to minimize χ^2. Especially in β-sheet secondary structure, intermolecular (centered around 1616-1627 cm^{-1} and 1697-1703 cm^{-1}) and intramolecular (centered around 1628-1637 cm^{-1}) β-sheet were calculated separately. The area of each peak has been taken as measure of the specific structure.

2.7. Amino acid composition

The amino acid composition of LM silk, silk cocoon and degummed silk was determined with the Waters AccQ-Fluor™ Reagent Kit using the AccQ-Tag™ amino acid analysis method (Waters Corp., Milford, MA, USA). For each sample, 4 mg was hydrolysed by 6 M HCl at 120 ± 2 °C in a silicone oil bath for 24 h. The air-dried hydrolysates were reconstituted with 20 mM HCl and then mixed with Waters AccQ-Fluor Reagent to obtain stable amino acids. The amino acid composition was determined by reverse phase high performance liquid chromatography (RP-HPLC) using an AccQ-Tag™ column (3.9 × 150 mm, Waters Corp., Milford, MA, USA) with a gradient of Waters AccQ-Tag™ Eluent A, Milli-Q water, and Acetonitrile (HPLC grade). The amino acids were detected with the Jasco UV-1570 detector set (Jasco, Bouguenais, France) at 254 nm. The chromatograms obtained were compared with Waters Amino Acid Hydrolysate Standards.

2.8. Cell culture

Murine embryo fibroblast (NIH 3T3, ATCC number: CRL-1658) cell line was cultured in Dulbecco's modified Eagle's medium (DMEM), with 10% fetal bovine serum (FBS), 1 mM sodium pyruvate, 2 mM L-glutamine and 1% antibiotic/antimycotic in a humidified atmosphere of 5% CO_2 at 37 °C with changing the medium every third day. Cells (at passage number 8) were collected by trypsin and were seeded in a 24-well plate (3×10^4 cells/well in 1.0 ml medium) with samples inside and cultured in standard NIH 3T3 medium. Before all the biological tests, samples were sterilized with aqueous ethanol solution 70% (v/v) for 2 h. After washed carefully to remove ethanol solution, samples were dried under a sterile hood at room temperature.

2.9. Cell morphology, distribution and immunofluorescence staining

Cell morphology and distribution were visualized by Rodhamine phalloidin and 4′6-diamidino-2-phenylindole (DAPI) staining. Rodhamine phalloidin stains actin filaments of cytoskeleton resulting in red fluorescence while DAPI stains nuclei resulting in blue fluorescence. At day 1 and day 2, the cell seeded samples were fixed with 4% paraformaldehyde, washed three times with PBS and then were permeabilized using 0.2% Triton X-100 PBS solution for 30 min. After washing in PBS for 3 times (15 min each time), cells were incubated with Rodhamine phalloidin (5.0 µl/well) and DAPI (1.0 ml/well, 5.4 µl dilute in 25.0 ml PBS) for 1 h at room temperature. After three rinses with PBS, samples were observed using Zeiss LSM 510 Meta confocal laser scanning microscope (CLSM).

2.10. Cell proliferation by DNA quantification (PicoGreen assay)

To evaluate cell proliferation on the different netwroks, a PicoGreen® DNA quantification assay (Quant-iT PicoGreen® dsDNA Assay, Invitrogen™, Carlsbad, USA) was used. After 1 and 2 days culture, the culture medium was removed and the samples were washed with PBS. Samples were then covered with 300 µl of 0.05% Triton-X in PBS, and the supernatants were collected and stored in single tubes (Eppendorf) at −20 °C until analysis. Before analysis, tubes were thawed at room temperature, and sonicated for 10 s with a Hielscher ultrasonic homogenizer (UP400S, 400 W-24 kHz, cycle 1, amplitude 40%, from Hielscher Ultrasonics, Teltow, Germany). Extracts of 100 µl were subsequently placed in a black 96-well plate, and mixed with 100 µl of PicoGreen® working solution, prepared following the manufacturer's instructions. Four independent samples were analyzed for each experimental condition. Fluorescence intensity was measured with a Tecan Infinite 200 microplate reader (Tecan Group, Männedorf, Switzerland) using excitation wavelength 485 nm and emission wavelength 535 nm. A calibration curve was created using a double-stranded DNA standard provided by the kit and was used for the calculation of the DNA content. Finally, the approximate number of cells per sample was determined from DNA content by the conversion factor of 7.7 pg DNA per cell.

2.11. Cell metabolic activity (AlamarBlue assay)

Cells viability after 1 and 2 days of culture was determined with AlamarBlue® Cell Viability assay (Invitrogen™, Carlsbad, USA), that quantifies cellular metabolic activity and in turn determines the concentration of viable cells in a given sample. AlamarBlue® reagent was added directly to each well 10% of the cell culture medium volume. Then, the well plates were incubated at 37 °C in a humidified atmosphere with 5% CO_2 for 45 min. A volume 100 µl of solution was collected from each well and the fluorescence signal was measured with a Tecan Infinite 200 microplate reader (Tecan Group, Männedorf,

Switzerland) with an excitation wavelength of 560 nm and an emission wavelength of 590 nm. Four replicates were considered for each experimental condition.

2.12. Statistics

In order to analysis the fracture strength distribution we used Weibull statistics. It is defined by the following relation

$$F(x, m, x_0) = 1 - e^{-\left(\frac{x}{x_0}\right)^m} \tag{1}$$

where x is the fracture strength m is the shape parameter and x_0 the scale parameter. F represents the probability that the sample break at the strength x.

In order to obtain the relative probability density distributions of the four different silk types (i.e. $f(x, m, x_o) = \frac{m}{x_0^m} x^{m-1} e^{-\left(\frac{x}{x_0}\right)^m}$) we obtained the Weibull shape and scale parameter by using the linear regression method. By applying the double logarithm to (1) we obtain the following equation

$$\ln\left[\ln\left(\frac{1}{1 - F(x)}\right)\right] = m\ln(x) - m\ln(x_0) \tag{2}$$

where F could be estimated through the median rank estimator

$$\hat{F}(x_i) = \frac{i - 0.3}{n + 0.4} \tag{3}$$

where n is the number of tested specimen and i is the order of the considered one (after the organization of the samples from the weakest till the strongest). Kolmogorov Smirnov test was performed to each seat of data to verify (under the 95% of acceptance, MatLab®) that Weibull statistics could be applied to data set.

For chemical characterizations, statistical evaluation was carried out using Origin Pro 2016 and Microsoft Office Excel 2010. Data were expressed as mean ± standard deviation (SD).

The *in vitro* NIH 3T3 cell proliferation and differentiation tests were performed on four replicates for each group. All quantitative data were expressed as mean standard ± deviation (SD). Statistical analyses were performed using GraphPad Prism 6 (GraphPad Software, La Jolla, CA, USA). The quantitative biological results were compared using a two-way analysis of variance (ANOVA). A significance level of 95% with a p value of 0.05 was used in all statistical tests performed.).

3. Results

3.1. Composition and structural characterizations

The results of amino acid composition analysis (mol %) of all samples (Table S1) showed remarkable differences between the composition of LM and silkworm silk, before (SC) and after (DS) degumming. In particular, LM silk presented much more Serine (23.0% vs. 11.2/11.7%) and much less Glycine (16.9% vs. 44.5/45.4%) and the presence of two amino acids, Asparagine (5.0%) and Glutamine (1.4%) are not found in the silkworm silk. By classifying amino acids into short chain (Gly, Ala and Ser) and long chain (Asp, Glu, Tyr, Arg, Leu, Val, Pro, Lys, Ile, Phe, Thr, Cys, His and Met) residues [33], LM presented more long chain residues (36.9% vs. 16.9/16.3%) and less short chain residues (63.0% vs. 83.1/83.7%).

Molecular structure of LM, SC and DS was characterized by Fourier Transform Infrared Spectroscopy (FTIR) (Fig. 2a). The peaks related to Amide A (3280 cm^{-1}), Amide I (1623 cm^{-1}), Amide II (1515 cm^{-1}) and Amide III (1230 cm^{-1}) were centered at the same wavelength [34]. In all silk samples, the peaks centered at around 1623 cm^{-1} (Amide I) and 1515 cm^{-1} (Amide II) indicated a significant amount of β-sheet structure [35]. A peak related to the presence of β-polyalanines was detected at 964 cm^{-1} just in LM spectra [36]. In order to better

elucidate the structure of protein in different samples, a secondary structure analysis was performed by analyzing the Amide I region (1600-1720 cm^{-1}) [37], and the results were summarized in Fig. 2b and c. LM fiber showed the lowest β-sheet (39.8% in total, 22.4% for intermolecular bonding) and α-helix (12.2%) structures with the highest random coils presence (27.6%). Among the other samples, DS showed the highest β-sheet (55.1%) content and lowest β-turn (13.5%).

3.2. Silk fibers morphology

Fibers morphology of different silks was observed by Field Emission Scanning Electron Microscopy (FE-SEM) (Fig. 3). FE-SEM images showed different surface morphologies and dimensions of the studied silks. LM silk (Fig. 3c) presented an irregular roughness that could be better seen at higher resolution in Fig. 3d. The fiber size calculated on FE-SEM images of SC and DS was in between 10 and 20 μm (Fig. 3a and b, respectively), while for LM silk (Fig. 3c) resulted less than 1 μm. The spontaneous assembling of silk filaments is also quite different, with isolable single fibers for SC and DS silks and regions of irregular assembling in LM filaments (Fig. 3c and d). Worth nothing is however the typical spigots of the *Linothele megatheloides* spider that are covered by scales, as shown in Fig. 1c.

3.3. Mechanical properties

Fig. 4 and Table S2 compare the tensile mechanical properties of the investigated silks. The mechanical properties of LM silk are very different from those of SC and DS (Fig. 4 and Table S2), with an elastoplastic behavior, a plastic onset at very small levels of stress and a failure that occurs with a progressive decrease of stress (Fig. 4a and b). The energy at break of LM silk was quite high, even if the smallest among the investigated fibers when normalized with respect to the volume (toughness: 4 ± 3 MJ/m^3 (LM), 82 ± 60 MJ/m^3 (SC), 55 ± 20 MJ/m^3 (DS)) (Table S2). On the other hand, by considering the computed Weibull parameters of these silks (Fig. 4c) and their relative distributions (Fig. 4d), we noticed huge differences in term of statistical behavior. In Weibull distributions of the strength (Fig. 4d), the narrower distribution highlights the more homogeneous behavior of this silk, untypical in spider silk that usually presents broader distributions.

3.4. Atomic Force Microscopy (AFM)

Atomic Force Microscopy (AFM) images obtained on the tested silks are reported in Fig. S2. In particular, *Linothele megatheloides* silk was the only one presenting submicrometric fibers diameter. The roughness data obtained from AFM images (Table S3) showed that LM presents the highest roughness (4.4 nm for Ra and 5.4 nm for Rq), confirming FE-SEM images. SC and DS had respectively the intermediate values of 1.9/2.6 nm, and 2.1/2.8 nm. All the tested fibers showed rather homogeneous surfaces with the exception of DS, in which numerous relief islands were visible and were probably due to presence of residual sericin spots (Fig. S2d).

Furthermore, AFM force/distance curves were used in order to measure adhesion of the cantilever tip on the silk surface, that, since the measurements were performed in air and were mainly influenced by the capillary forces, so, the tract where the tip detaches from the sample, can be considered a qualitative indicator of the surface wettability (Fig. S3). The shapes of the curves were significantly different among the samples and the values of the adhesion force necessary to detach the tip from silk surfaces (snap-out) are reported in Table S4. In particular, since the z travel range of the used scanner was limited to 4 μm, for LM silk type it was not able to finalize the snap-out of the tip from the surface. This sets the sample at the highest level of adhesion force among all the others. The high standard deviation obtained on DS with respect to the other samples could be correlated with the presence of
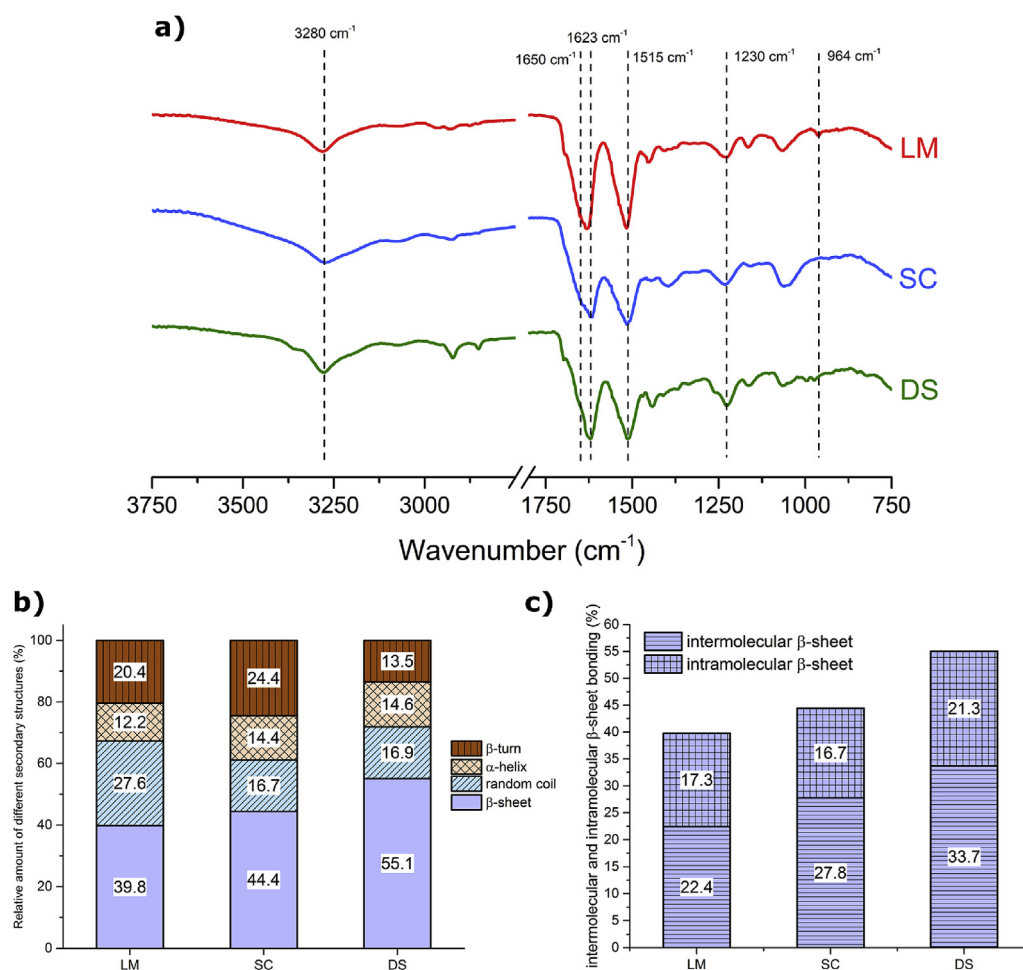
Fig. 2. Molecular structure analyses. a) Samples FTIR spectra; b) FTIR secondary structure analysis on Amide I of different silks (based on related structure peak areas); c) Ratio of intermolecular and intramolecular bonds detected on different silks (based on related intermolecular and intramolecular β-sheet areas). LM: *Linothele m.* silk; SC: *Bombyx m.* silk; DS: degummed *Bombyx m.* silk.

highly hydrophilic sericin spots (Fig. S3d) that could strongly scatter the adhesion values.

3.5. Cell proliferation and metabolic activity on different natural networks

To investigate the early stage of interaction of the investigated silks with cells, NIH 3T3 cell line were seeded on the network naturally produced by spider (LM) and derived from the silk of the silkworm cocoon (SC and DS), prepared as reported in the materials paragraph. Cell proliferation studies were performed at day 1 and day 2, using PicoGreen® DNA quantification assay. According to the results (Fig. 5a), cell number of each sample increased gradually at each time point. However, LM silk had the largest number of adhered cells during two days' cell culture; while the increasing of the cells in day 2 was not as significant as SC and DS. These results were in well agreement with the confocal images (Fig. 5g – l) that evidenced a larger cell growth for LM silk network than for other networks. It was obvious from Fig. 5g – l that cells adhered on LM silk maintained the regular spindle shaped cellular morphology and were well connected to each other after 2 days culture in comparison to as in SC and DS.

Fig. 5b and c reports the NIH 3T3 cells metabolic activity, measured

by AlamarBlue® assay. For LM silk, the total cellular metabolic activity was significantly higher than other samples, but showed no sensible increment from day 1 to day 2. DS promoted a continuous increasing of cell metabolic activity while SC showed a decrease. Total cell metabolic activity was also normalized to total DNA content previously determined using the PicoGreen® DNA quantification assay (Fig. 5c). Cells seeded on LM silk showed a higher specific activity when compared to others in all time points. Nevertheless, SC showed a lower normalized activity than DS in day 2.

3.6. Cell adhesion, morphology and distribution on different silk fibers

Single fiber competitive combinations of LM silk with SC and DS, arranged as indicated in Fig. 6, were set for NIH 3T3 adhesion tests. Confocal microscopy images (Fig. 6) clearly indicated that already at day 1 the LM silk filaments were fully covered by well spread cells, forming clusters, with only a few or no cells adhering to the other samples, even after two days culture. The findings are confirmed by FE-SEM images of Fig. 6, moreover indicating a high degree of spreading of cells on LM fibers and the presence after two days of a continuous cell monolayer, in particular when in competition with SC fibers (Fig. 6l).
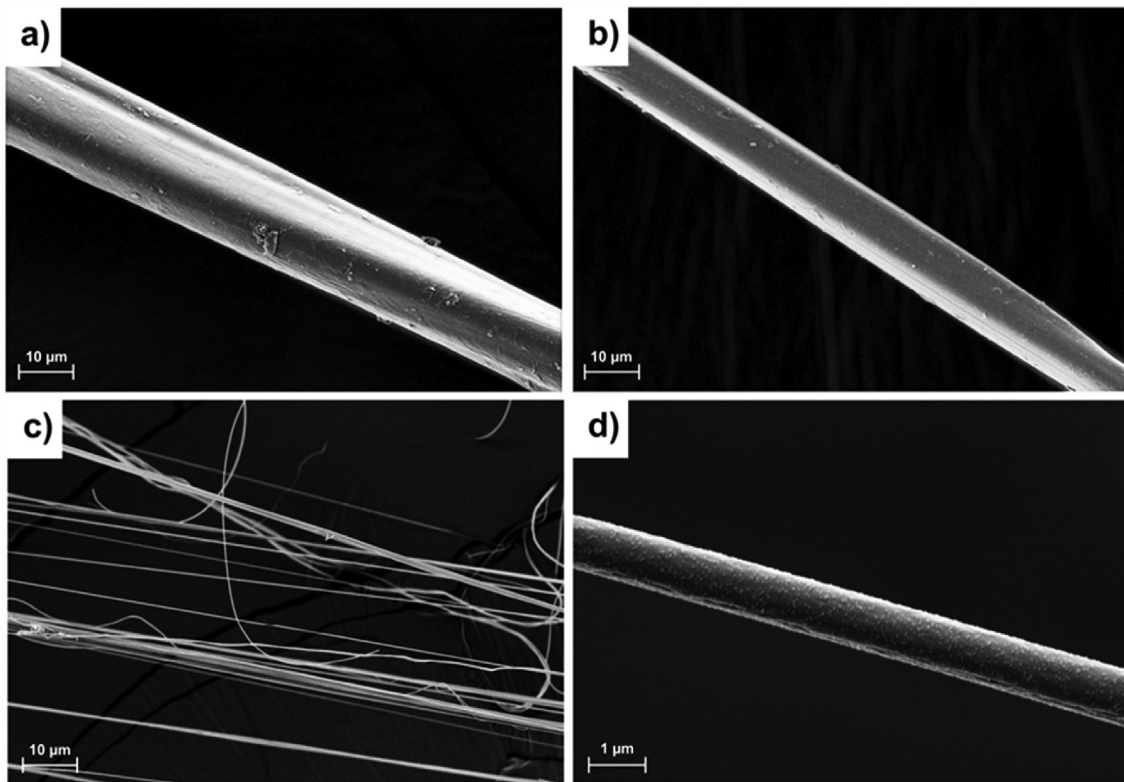
Fig. 3. FE-SEM images of silk fibers. a) Silkworm cocoon silk from *Bombyx mori* before (SC) and b) after degumming (DS); c) and d) *Linothele megatheloides* spider silk (LM) in different magnifications. The scale bars in figure a, b and c are equivalent to 10 μm and the scale bar in figure d is equivalent to 1 μm.

4. Discussion

Silks are a family of proteins, that can be produced by several organisms like Lepidoptera and Arthropods [38]. Depending on source,

silks can be very different in terms of chemistry, molecular structure and mechanical properties [16]. The domestic silkworm *Bombyx mori* silk has been deeply studied, worldwide used for making fabrics, employed in surgery already in the past as suture thread and more recently
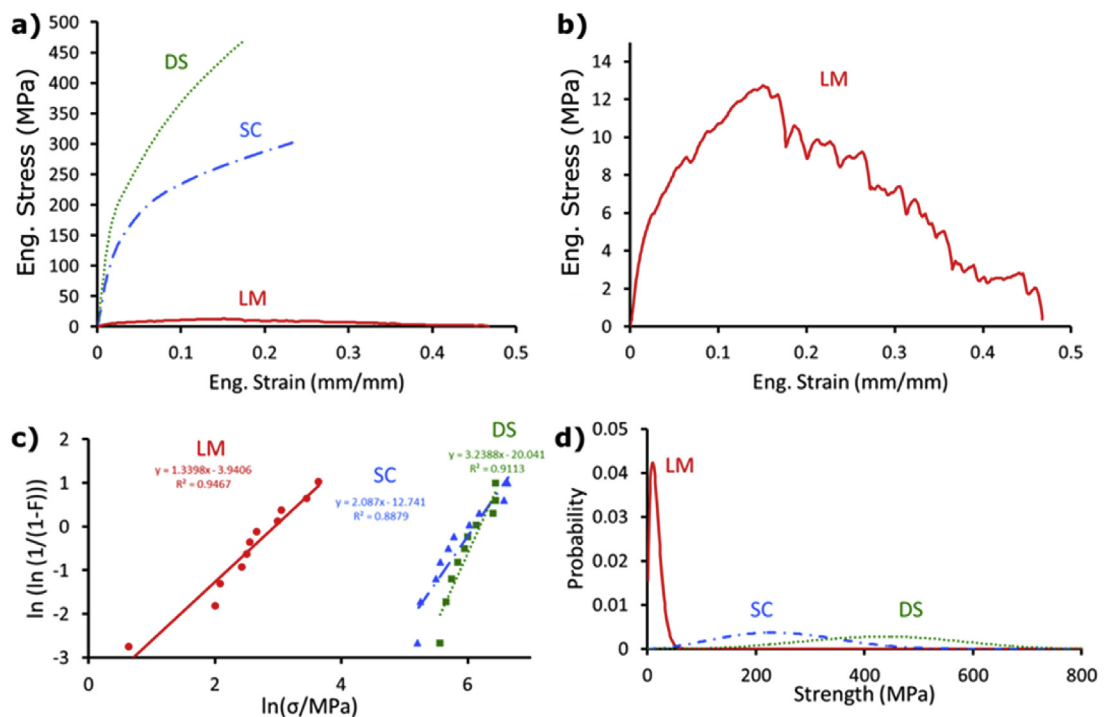

Fig. 4. Mechanical behaviors of samples. a) the tested different silks; b) LM silk. c) Linear regression method used to compute the Weibull parameters and d) Weibull probability distribution of the strength of the tested silks. LM: *Linothele m.* silk; SC: *Bombyx m.* silk; DS: degummed *Bombyx m.* silk.
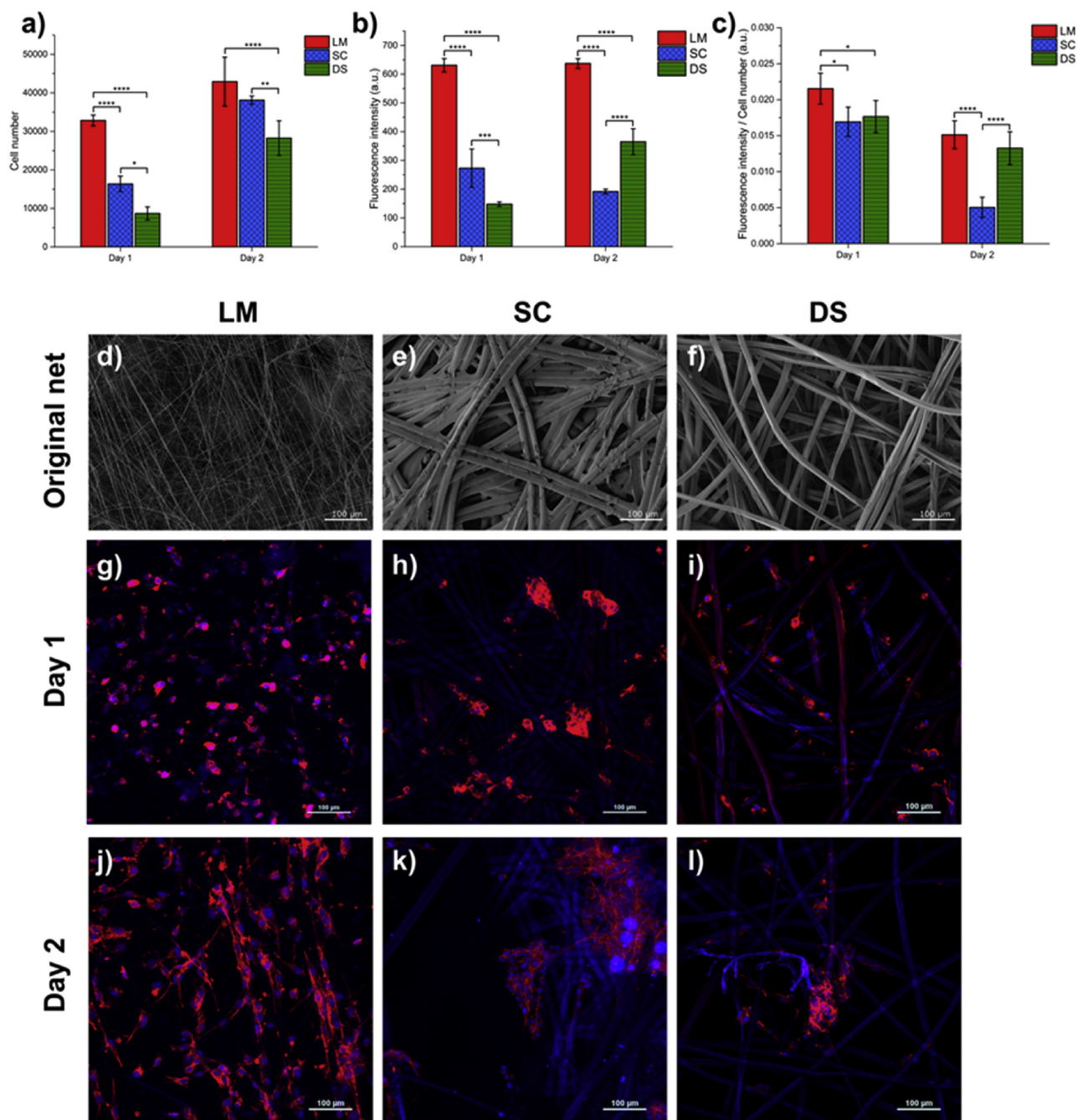
Fig. 5. Cell adhesion, proliferation and metabolic activity for NIH 3T3 cell line cultured for 1 and 2 days on different silk network. a) cell number derived from total DNA content measured by PicoGreen assay; b) total metabolic activity determined by AlamarBlue assay; c) metabolic activity normalized with respect to DNA content. d) - f) FE-SEM images of different original silk networks (without cells), and g) - l) confocal microscopy images of samples seeded with NIT 3T3 after day 1 and day 2 of culture. LM: *Linothele m.* silk; SC: *Bombyx m.* silk; DS: degummed *Bombyx m.* silk. The Scale bars in the figures are equivalent to 100 μm.

proposed for the repair of tendons and ligaments and for the fabrication of tissue engineering scaffolds [5–9]. Nowadays, also spider silk is draining the attention of scientists working in biomedical field [4].

In our work, for the first time, we have characterized physical and biological properties of *Linothele megatheloides* (LM) spider, produces a single type of silk in a relatively quite large quantity (60 mg/week), which partially overcomes the limitations of silk procurement from other types of spiders. LM silk was compared with the already deeply investigated silk filament of *Bombyx mori* silkworm. Samples were evaluated in terms of chemical (amino acid composition, FTIR and secondary analysis) and physical (AFM, tensile test and morphology

observation) properties. Finally, cell adhesion, metabolic activity and purification were investigated by culturing NIH 3T3 cells on the different silk fibers and networks. The results were assessed by imaging (confocal microscopy and FE-SEM) and quantitative analysis (AlamarBlue and PicoGreen assay).

Amino acid composition is one of the most important aspects considering the impact on secondary structure, molecular water interaction and, as a consequence, on mechanical properties. Results demonstrated a remarkable difference in amino acid composition between LM silk and the other samples. Gly, Ala and Ser were the most abundant amino acids in all considered silks types, and all were involved in β-sheet
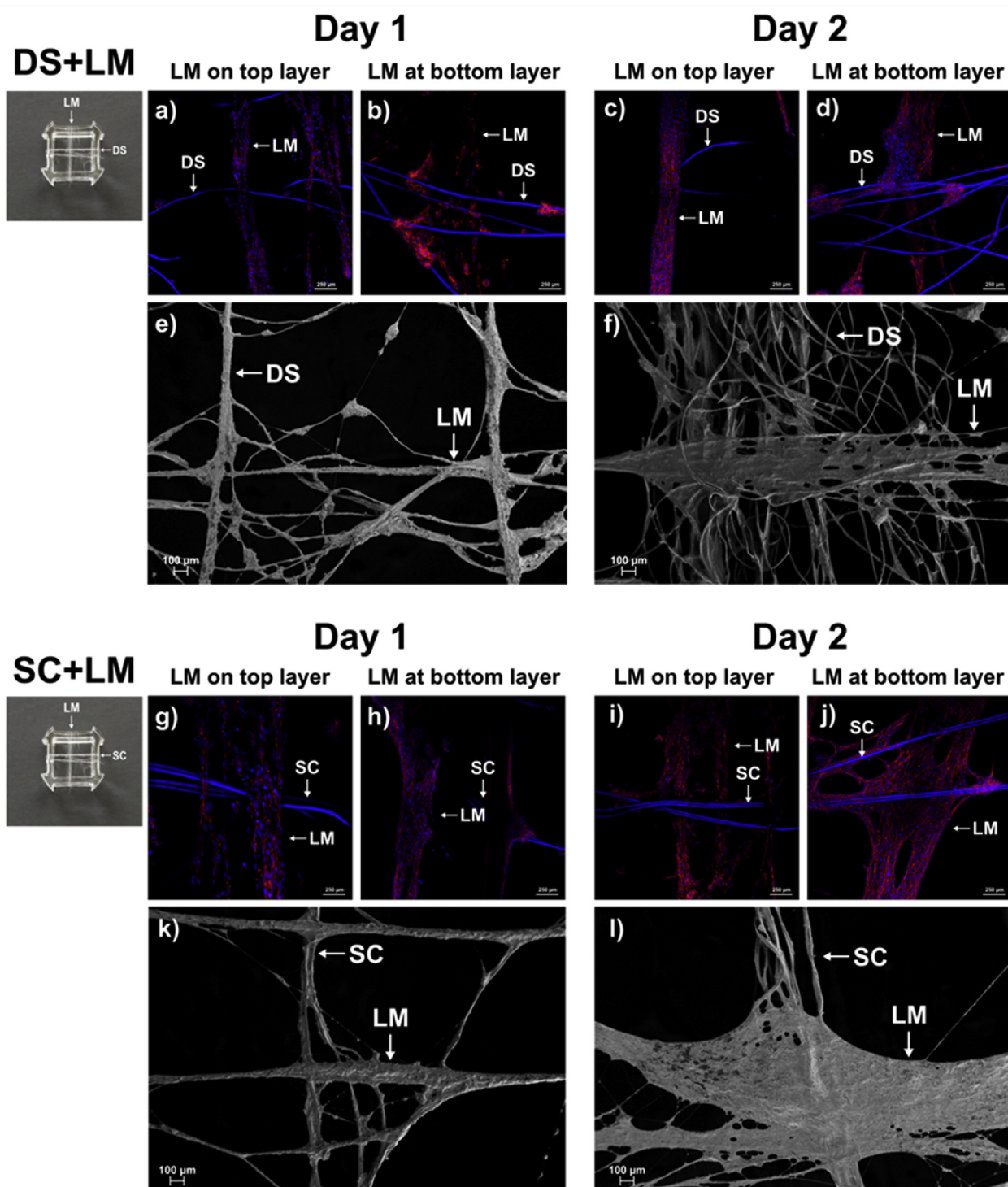
Fig. 6. Cell adhesion, morphology and distribution on different silk fibers. a) - d) and g) - j) Confocal images of NIH 3T3 cells adhesion on different silks samples at day 1 and day 2 of culture. The scale bars in the figures are equivalent to 250 μm. e) - f) and k) – l) FE-SEM images of cell adhesion on different silks samples after day 1 and day 2 of culture. The scale bars in these figures are equivalent to 100 μm. LM: *Linothele m.* silk; SC: *Bombyx m.* silk; DS: degummed *Bombyx m.* silk.

secondary structure formation [33]. However, it was observed that the composition of different types of silk differ mainly in the relative percentages of individual residues, and also, in the presence/absence of specific residues (rich in Glu and Asp). By classifying protein residues into short chain (S) and long chain (L), it is worth noticing that the lowest percentage of S residues increases the ratio of L/S in LM silk. The lowest amount of short side residues, together with the lowest content of Gly makes LM silk fibers less able to structure in β-sheets. In fact, the

lowest content of β-sheet was detected in LM silk together with highest random coils conformations. This conformation defined a more flexible material with a higher extensibility (Fig. 4) with respect of the other samples. In addition, intramolecular bonding (stabilize the secondary structure of the chain) and intermolecular bonding (forces between chains holding in a substance) also effect the mechanical properties. As expected from the amino acid composition, LM silk fiber had the lowest content of intermolecular bonds, due to the lowest percentage of Gly,

which also played a role on tensile behavior (Fig. 4a).

Under tensile testing, LM silk behaves in a different way with respect to other typical silks, with a more softening rather than stiffening constitutive law (Table S2). The softening - often associated to stress drops - is correlated to the failure of single fibers within the thread sample [39], which in this case is basically a bundle of fibers. This result was also in well agreement with the results of secondary structure analysis: the lower amount of β-sheets (low intermolecular bonding) present in LM silk, leads to a lower strength (16 ± 10 MPa) and toughness (4 ± 3 MJ/m^3) of the material. The group of fibers that composed a single sample did not simultaneously break under load (Fig. 4b) and the stress drop was progressive and not catastrophic as in the other cases (when break occurs). The surface roughness was observed by FE-SEM imaging (Fig. 3) and confirmed by AFM analyses. The highest roughness of LM silk could be attributed to a different way of fiber production by the three considered animals. *Linothele megatheloides* spins many tiny and sticky fibers per time (Figs. 1b and 3c), leading to a high difficulty in isolating a single thread without damaging it.

To evaluate the bioactivities of different silks in terms of cell adhesion, proliferation and metabolism, natural networks were taken into consideration firstly. The cells adhered on LM network demonstrated a significant enhancement of cell number, a higher cellular proliferation and metabolic activity comparing to other samples. This trend was confirmed also by normalized metabolic activity. Interestingly, cells adhered on DS showed a slower proliferation and activation compare with LM in day 1, but after 2 days became comparable. The different cell behavior was observed on SC and DS due to the release of sericin from SC, which was already seen to promote fast cell adhesion and with a mitogenic effect on cells (for example, corneal epithelial cells and retinal cell [40]). These results were in well agreement with cell adhesion morphology. In general, cell behavior was not affected by the position of silk in the samples (LM on top or bottom), but mainly by the silk type. Well spared and regular spindle shaped cellular morphology were observed on LM silk in comparison to lower affinity globular clusters. The preliminary NIH 3T3 cell adhesion evaluation clearly showed the highest cell adhesion ability on LM silk fibers.

Cell adhesion is a complex mechanism, driven by several aspects, mostly controlled by hydrophilicity, surface chemistry and material morphology, and depending on the adhesion mechanisms, different cell activities can be triggered [41]. Environment stored fibers contained alike amount of water, in the range 7–8.5%, as determined by thermogravimetric analysis (data not reported here). This can suggest that they will take comparable amount of water when immersed in the culture medium, that would be however impossible to measure without introducing artifacts in the experiment.

The LM fibers lowest relative amount of β-sheet (intermolecular bonding) and the highest amount of random coils together with a very high roughness, can well explain the fast cell adhesion observed. Furthermore, a contribution on early adhesion could come from the different fiber size in the nets [42]. We have demonstrated that LM silk stimulated NIH 3T3 cells proliferation after one day and two days of *in vitro* culture. It was confirmed the faster cell adhesion and activation on LM when compared with *Bombyx m.* silk, in particular in the early stage (1 day). The results suggested that the silk of *Linothele megatheloides* can induce a faster cell adhesion and activation in comparison to the other tested fibers. Considering that *Linothele megatheloides* produces a single type of silk, with high homogeneity and relatively high production rate, it can be considered as a potential source for developing novel spider silk based materials from nature.

5. Conclusions

Chemical, mechanical and *in vitro* biological properties of *Linothele megatheloides* spider (LM) silk were determined in comparison with *Bombyx mori* silkworm silk, before and after degumming. LM silk is characterized by the fact that it produces for the network just one type of filament at a relatively high production rate when compared to other spiders, this making easier the collection and evaluation of this silk for potential applications also in medicine. With respect to the *Bombyx mori* silkworm silk (before and after degumming), LM silk presented higher amount of serine in amino acid composition, lower amount of β-sheet and α-helix secondary structure and higher random coils units. Moreover LM fibers were thinner (less than 1 μm diameter), rougher, and resulted to have the highest level of adhesion force among all the tested samples. NIH 3T3 cells were used to evaluate the early stage of cell adhesion *in vitro* biological properties of the investigated silks. A first used specific setup with couples of fibers arranged in competitive arrays, demonstrated the highest early time cell adhesion of the LM silk. These results have been confirmed by cell culture tests on samples made from the nets or from the cocoons, where again faster cellular proliferation together with a more proficuous metabolic activity was confirmed for LM silk samples. The noticeable biological behavior of LM silk found in these preliminaty tests justifies further and deeper investigations in order to outline hypotheses on the its potential use for applications in biomedicine and namely in the field of tissue engineering.

Author contributions

Yuejiao Yang, Gabriele Greco, Claudio Migliaresi, Nicola Pugno and Antonella Motta conceived the idea of the experiment. Experimental data were taken by Yuejiao Yang, Gabriele Greco, and Devid Maniglio. Data analysis was performed by Yuejiao Yang, Gabriele Greco, Devid Maniglio, Claudio Migliaresi, Nicola Pugno and Antonella Motta. The paper was written by Yuejiao Yang, Gabriele Greco, Devid Maniglio, Claudio Migliaresi and Antonella Motta with input from all authors. All authors have given approval to the final version of the manuscript.

Declaration of competing interest

None.

Appendix A. Supplementary data

Supplementary data to this article can be found online at https://doi.org/10.1016/j.msec.2019.110197.

Abbreviations

LM	*Linothele megatheloides*
SC	*Bombyx mori* cocoon
DS	Degummed *Bombyx mori* cocoon

FE-SEM   Field Emission Scanning Electron Microscopy
FTIR   Fourier Transform Infrared Spectroscopy
AFM   Atomic Force Microscopy

References

[1] Z. Shao, F. Vollrath, Nature 418 (2002) 741-741.
[2] S.W. Cranford, A. Tarakanova, N.M. Pugno, M.J. Buehler, Nature 482 (2012) 72–76.
[3] O. Hakimi, D.P. Knight, F. Vollrath, P. Vadgama, Compos. B Eng. 38 (2007) 324–337.
[4] H.M. Tahir, K. Zahra, A. Zaheer, K. Samiullah, Punjab Univ. J. Zool. 32 (2017) 143–154.
[5] P. Bhattacharjee, B. Kundu, D. Naskar, H.-W. Kim, T.K. Maiti, D. Bhattacharya, S.C. Kundu, Acta Biomater. 63 (2017) 1–17.
[6] D. Jao, X. Mou, X. Hu, J. Funct. Biomater. 7 (2016) 22.
[7] C. Migliaresi, A. Motta, Scaffolds for Tissue Engineering: Biological Design, Materials, and Fabrication, Pan Stanford, 2014.
[8] T. Yucel, M.L. Lovett, D.L. Kaplan, J. Control. Release 190 (2014) 381–397.
[9] K. Numata, D.L. Kaplan, Adv. Drug Deliv. Rev. 62 (2010) 1497–1508.
[10] K. Gellynck, P. Verdonk, R. Forsyth, K.F. Almqvist, E. Van Nimmen, T. Gheysens, J. Mertens, L. Van Langenhove, P. Kiekens, G. Verbruggen, J. Mater. Sci. Mater. Med. 19 (2008) 2963–2970.
[11] N.M. Pugno, S.W. Cranford, M.J. Buehler, Small 9 (2013) 2747–2756.
[12] A. Meyer, N.M. Pugno, S.W. Cranford, J. R. Soc. Interface 11 (2014) 20140561.
[13] O. Hakimi, D.P. Knight, M.M. Knight, M.F. Grahn, P. Vadgama, Biomacromolecules 7 (2006) 2901–2908.
[14] N.M. Pugno, Meccanica 53 (2018) 1105–1114.
[15] R.B. Suter, J. Arachnol. (1992) 107–113.
[16] T. Asakura, T. Miller, Biotechnology of Silk, Springer, 2014.
[17] A. Basu, Advances in Silk Science and Technology, Woodhead Publishing, 2015.
[18] C. Allmeling, A. Jokuszies, K. Reimers, S. Kall, C. Choi, G. Brandes, C. Kasper, T. Scheper, M. Guggenheim, P. Vogt, Cell Prolif 41 (2008) 408–420.
[19] F. Vollrath, P. Barth, A. Basedow, W. Engström, H. List, In vivo (Athens, Greece) 16 (2002) 229–234.
[20] M.C. Andrade, Behav. Ecol. 9 (1998) 33–42.
[21] J. Scheller, U. Conrad, Mol. Farming: Plant-made Pharm. Tech. Proteins 11 (2006) John Wiley & Sons.
[22] A. Salazar, M. Keusgen, J. von Hagen, Amino Acids 48 (2016) 1161–1171.
[23] F. Teulé, Y.-G. Miao, B.-H. Sohn, Y.-S. Kim, J.J. Hull, M.J. Fraser, R.V. Lewis, D.L. Jarvis, Proc. Natl. Acad. Sci. 109 (2012) 923–928.
[24] H. Chung, T.Y. Kim, S.Y. Lee, Curr. Opin. Biotechnol. 23 (2012) 957–964.
[25] C.H. Bowen, B. Dai, C.J. Sargent, W. Bai, P. Ladiwala, H. Feng, W. Huang, D.L. Kaplan, J.M. Galazka, F. Zhang, Biomacromolecules 19 (2018) 3853–3860.
[26] A. Rising, J. Johansson, Nat. Chem. Biol. 11 (2015) 309.
[27] M. Andersson, Q. Jia, A. Abella, X.-Y. Lee, M. Landreh, P. Purhonen, H. Hebert, M. Tenje, C.V. Robinson, Q. Meng, Nat. Chem. Biol. 13 (2017) 262.
[28] N. Paz, R.J. Raven, J. Arachnol. (1990) 79–86.
[29] W.G. Eberhard, N.A. Hazzi, J. Arachnol. 41 (2013) 70–75.
[30] F. Vollrath, Int. J. Biol. Macromol. 24 (1999) 81–88.
[31] T.A. Blackledge, J.E. Swindeman, C.Y. Hayashi, J. Exp. Biol. 208 (2005) 1937–1949.
[32] C. Boutry, T.A. Blackledge, J. Exp. Biol. 213 (2010) 3505–3514.
[33] S.J. Lombardi, D.L. Kaplan, J. Arachnol. (1990) 297–306.
[34] E. Metwalli, U. Slotta, C. Darko, S. Roth, T. Scheibel, C. Papadakis, Appl. Phys. A 89 (2007) 655–661.
[35] E. Cooper, K. Knutson, Fourier transform infrared spectroscopy investigations of protein structure, Physical Methods to Characterize Pharmaceutical Proteins, Springer, 1995, pp. 101–143.
[36] K. Spiess, R. Ene, C.D. Keenan, J. Senker, F. Kremer, T. Scheibel, J. Mater. Chem. 21 (2011) 13594–13604.
[37] X. Hu, D. Kaplan, P. Cebe, Macromolecules 39 (2006) 6161–6170.
[38] C.L. Craig, Annu. Rev. Entomol. 42 (1997) 231–267.
[39] N.M. Pugno, T. Abdalrahman, Nanosci. Nanotechnol. Lett. 3 (2011) 882–884.
[40] Z. Wang, Y. Zhang, J. Zhang, L. Huang, J. Liu, Y. Li, G. Zhang, S.C. Kundu, L. Wang, Sci. Rep. 4 (2014) 7064.
[41] H.-I. Chang, Y. Wang, Cell responses to surface and architecture of tissue engineering scaffolds, Regenerative Medicine and Tissue Engineering-Cells and Biomaterials, InTech, 2011.
[42] A.T. Nguyen, S.R. Sathe, E.K. Yim, J. Phys. Condens. Matter 28 (2016) 183001.